

# Postural Balance of Kneeling Gaits on Inclined and Elevated Surface for Construction Workers

Siyu Chen, Yi Yu, Chong Di, Duncan T. Stevenson, Mitja Trkov, Jie Gong, and Jingang Yi

**Abstract**—We present a human postural balance study on quiet stance and kneeling gaits on inclined and high elevated surfaces for construction workers. To simulate the high elevation, an immersive mixed reality environment is built with an actual inclined roof surface to create somatosensory haptic feedback. We quantify the postural balance during quiet kneeling and stance through measurements of the center of pressure and sway motion of the upper-body under various inclined angles and heights. The results of center of pressure and trunk acceleration measurements show smaller postural sway during kneeling compared to standing. A mathematical model is also presented to help understand the experimental results and potentially provide design guidance for further intervention to prevent and mitigate the fall risk for construction workers. The model and controller parameters are optimized to precisely capture and explain the experimental results.

## I. INTRODUCTION

Construction industry is one of the highest-risk private sectors in the US, contributing for 21.6% of all the fatal injuries in industry in 2019 [1]. Among all fatal injuries, roofer is the leading construction trade and has the fourth highest fatal work injury rate among all occupations [1], [2]. Roofers perform more than 66% of their working time in kneeling, crouching, stooping, or crawling postures or gaits at high elevation and inclined surfaces [3]. It is important to understand the human postural balance control of kneeling gaits on inclined and elevated surfaces and thus to possibly introduce interventions to prevent and mitigate fall risk.

Many environmental factors influence postural balance control of construction workers such as elevation, visual scenes, inclined and restricted support surfaces [2]. Although study of human quiet stance has been reported extensively (e.g., [4], [5]), limited research exist on postural control of kneeling gaits on elevated or inclined surfaces. In [6], quiet kneeling is studied and compared with the stance with eye-open and eye-closed. Center of pressure (COP) motion and power spectral density (PSD) are used as a means to identify the difference between kneeling and stance gaits. The results in [6] conclude that PSD under kneeling shows significant difference with stance and visual feedback plays

a significant role on the COP motion under kneeling gaits. However, neither elevation nor inclined kneeling surface was considered.

Understanding and studying postural balance of quiet stance on elevated and inclined surfaces have been reported [7]–[9]. In [7], the human subject experiments were conducted in real environment and the elevation is only 61 cm above the ground. In [8], [9], virtual reality (VR) was used as a tool to generate the high elevation and environmental scenes since running human subject experiments in high elevation location is unsafe, inconvenient and expensive. No difference was reported among the experimental outcomes in terms of height effects on human quiet stance between real and VR environments and therefore, VR or augmented reality (AR) environments is a popular tool to study human behaviors in elevation [10]. Indeed, virtual reality, augmented reality and mixed reality (MR) become an important emerging technology for construction safety and trade skills training [10]–[14]. For example, it is promising to use an integrated VR and motion capture devices to study social learning among construction workers for fall risk behaviors in high elevation [15].

In this paper, we study the postural balance of kneeling gaits on inclined and elevated surfaces for construction workers. We use the mixed reality setup to construct the high elevation and visual scenes while subjects conduct kneeling gaits on a real inclined roof surfaces. Wearable inertial measurement units (IMUs) are used to obtain the human upper trunk acceleration to quantify the body sway in sagittal and frontal planes. Quiet stance is conducted and compared with the kneeling gait results. We also use the inverted pendulum model and neuro-controller to analyze the balance performance for both quiet stance and kneeling gaits. Optimization process of model parameters is performed for the individual test and results show close matching between the power spectral density of the experimental and model prediction center of pressures. The main contribution of this work lies in the use of MR and analytical models to study the postural balance of kneeling gaits on elevated and inclined surfaces. Comparing with the quiet stance, this work complements the existing results and studies on quiet stance by providing new results in kneeling gaits. Comparing with the kneeling studies in [6], we mainly focus on the influence of elevation and inclined surfaces on balance performance. The outcomes of this work would potentially provide guidance to further design knee or hip robotic assistive intervention for kneeling gaits [16]–[19].

The work was supported in part by the US NSF under award IIS-2026613. S. Chen and J. Yi are with the Department of Mechanical and Aerospace Engineering, Rutgers University, Piscataway, NJ 08854 USA (e-mail: siyu.chen@rutgers.edu; jgyi@rutgers.edu).

Y. Yu, C. Di and J. Gong are with the Department of Civil and Environmental Engineering, Rutgers University, Piscataway, NJ 08854 USA (e-mail: yi.yu.civil@rutgers.edu; chong.di29@rutgers.edu; jg931@soe.rutgers.edu).

D.T. Stevenson and M. Trkov is with the Department of Mechanical Engineering, Rowan University, Glassboro, NJ 08028, USA. (e-mail: stevensod8@students.rowan.edu, trkov@rowan.edu).

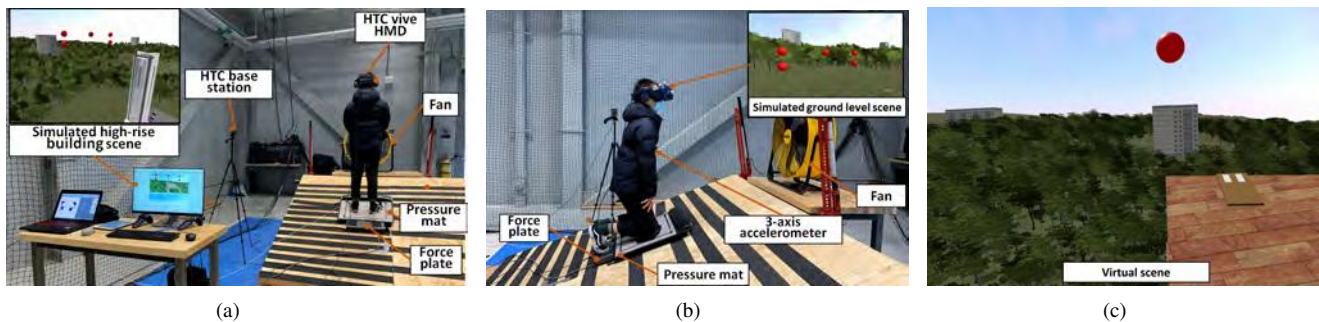


Fig. 1. Mixed reality experimental setup on slope surface (a) standing, (b) kneeling. (c) The virtual scene that the subjects see from the VR headset.

## II. MR-ENHANCED BALANCE EXPERIMENTS

### A. Experiment Design

We built an adjustable tilting virtual roof platform with wooden planks, which was combined with a VR system to build an MR environment. A backpack-type portable computer with HTC Vive Pro VR system was used in the experiments. With the backpack computer, the experimental system enables users to wear the equipment without tethering. The VR environment is built with the Unity game engine and it can stream subject's motion through motion tracking system. In order to provide a realistic virtual testing scenario, the spatial information of the room and simulated roof platform geometry were captured by a static LIDAR scanner. The virtual scenario on high (rooftop of a high-rise 30th floor building) and low elevated surface (ground) were constructed. The VR world was aligned with physical environment before the start of each tests.

In the virtual environment, both high and low elevated surface scenes are simulated to provide the test subject with different virtual immersive experience. Fig. 1(a) shows the subject standing on top of the sloped rooftop platform while observing the simulated high-rise building scene. Fig. 1(b) shows the subject kneeling on sloped surface while observing the simulated ground scene. To simulate realistic high-rise building environment, a fan was placed in front of the subject to generate strong wind and wind noise sound was played from the headset. Different test conditions were combined and used such as standing/kneeling, level/sloped surface and high/low elevated virtual environment.

### B. Experimental Protocol and Data Process

Three young healthy subjects ( $n = 3$ , age:  $28.3 \pm 2.9$  years, weight:  $69.2 \pm 13.8$  kg, height:  $169.3 \pm 9.3$  cm) with no known musculoskeletal or neurological defects were recruited for this study. All participants were informed about the testing protocol and signed the informed consent forms approved by the Institutional Review Board (IRB) at Rutgers University.

The participants were asked to perform quiet standing and kneeling tasks on a level (0 deg) and sloped (20 deg) surface. Visual perturbations were induced by changing the scene of the virtual environment. In addition, a sudden perturbation simulating strong wind conditions were induced using a strong fan aimed at subjects' upper trunk after first 30 sec

of subjects balancing. Subjects were instructed to keep their balance and follow the visual tasks/targets (i.e., red dots in front of the subject) in the simulated environment. During tests, the subjects were instructed to kneel down or step on the force plate for each testing condition and keep their balanced for 60 sec. First 10 sec of data acquisition in each test were discarded. Overall, the subjects performed the following tasks: standing or kneeling on 0 deg, and standing or kneeling on 20 deg.

In the experimental setup,  $x$ -,  $y$ -, and  $z$ -axis are defined as anterior-posterior (A-P), medial-lateral (M-L), and upward-downward (U-D) direction respectively. A 3-axis accelerometer (BWT901CL, WitMotion Inc.) was strapped on subjects' chest to record postural sway accelerations in the A-P,  $\ddot{x}_{COM}$ , and M-L,  $\ddot{y}_{COM}$ , directions. The portable force plate (Berotec Corporation.) and pressure mat (MatScan, Tekscan Inc.) were used to collect ground reaction forces/torques and pressure distribution measurements under feet on sloped and level surfaces. Vicon motion capture system (8 Vantage cameras, Vicon Motion Systems Ltd.) was used to collect positions of subjects' feet and pressure mat. Data from all sensors was synchronized and collected at 100 Hz on a portable high-performance micro-processor (Intel NUC7i7DNK, Intel Corp.) through wireless connection.

Data from the force plate were used to evaluate the sway of the center of pressure in A-P and M-L directions, denoted as  $CP_x$  and  $CP_y$ , respectively. Several metrics were used to determine the postural balance stability. The power spectral density (PSD), root mean square (RMS), and mean velocity (MV) of  $CP_x$  and  $CP_y$  measurements were computed for all trials across all test conditions. The PSD was calculated using Welch method [6] with 2000 samples per periodogram and a spatial resolution of 0.05 Hz. The RMS was defined as  $RMS = \sqrt{\frac{1}{N} \sum_{n=1}^N x_i^2}$ , and MV was calculated as  $MV = \frac{f_s}{N} \sum_{n=2}^N |x_i - x_{i-1}|$ , where  $N$  is the number of samples of signal  $x_i$  and  $f_s$  is the sampling frequency. Characteristics of the postural sway using the accelerometer measurements,  $\ddot{x}_{COM}$  and  $\ddot{y}_{COM}$ , were analyzed based on the 95% ellipse of postural acceleration sway [20] (major axis, minor axis, and sway area). The RMS of the  $\ddot{x}_{COM}$  and  $\ddot{y}_{COM}$  were computed to analyze the variability of corrective movement of the center of mass. In addition, we analyzed the experimental torque  $T_c$  measurements which were normalized with the body mass.

### III. NEURAL POSTURAL BALANCE CONTROL

#### A. Neural Balance Controllers

We consider an inverted pendulum model for human body sway in the sagittal plane during the quiet stance and kneeling balances. Fig. 2 shows the schematic of the inverted pendulum models for stance and kneeling gaits. The pendulums pivot around point  $O$  on the tilted surface. We denote the human body tilted angle and sloped angle as  $\theta_b$  and  $\theta_s$ , respectively. The distances from the human mass center to foot and knee are denoted as  $h_s$  and  $h_k$ , respectively. The mass and mass moments of inertia for stance and kneeling gaits are denoted as  $m_s$  and  $J_s$ ,  $J_k$ , respectively. Fig. 3 illustrates the block diagram of the human postural neural balance control model. The model is adopted from the development in [6] and [5] for quiet kneeling and stance, respectively.

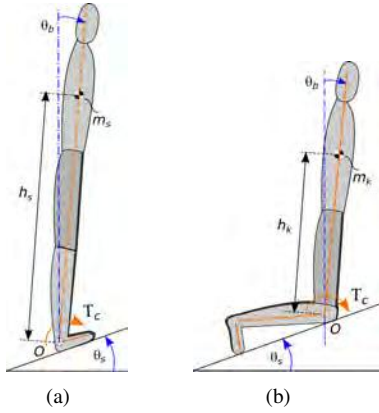


Fig. 2. Inverted pendulum model for a) standing, b) kneeling on slope surface.

For inverted pendulum sway in the sagittal plane with small magnitude of  $\theta_b$ , we obtain the equation of motion as

$$J_s \ddot{\theta}_b + m_s g h_s \theta_b = T_c, \quad (1)$$

where  $T_c$  is the total torque applied on the human body. Denoting the positions of the mass center (COM) and COP in the horizontal plane as  $x_{\text{com}}$  and  $CP_x$ , respectively, we obtain

$$x_{\text{com}} = h_s \theta_b, \quad CP_x = x_{\text{com}} + \frac{J_s}{m_s g h_s} \ddot{x}_{\text{com}}. \quad (2)$$

From (1) and (2), we obtain the transfer function from  $CP_x$  to  $\theta_b$  as

$$\frac{CP_x(s)}{\Theta_b(s)} = \left(1 + \frac{J_s s^2}{m_s g h_s}\right) h_s. \quad (3)$$

For neural balance postural control, as shown in Fig. 3, we consider vision, vestibular and proprioceptive sensory feedback. The vision and vestibular sensory is considered into one feedback loop with a combined gain  $W_{\text{vv}}$ . The proprioceptive sensory feedback is modeled with gain  $W_{\text{prop}}$  and composite tilted angle  $\theta_b - \theta_s$ . The neural controller contains the time delay  $\tau$  and the PID module  $C_n(s) = K_p + K_d s + \frac{K_i}{s}$ . The passive mechanism is modeled  $P(s) = K_{ps}$ .

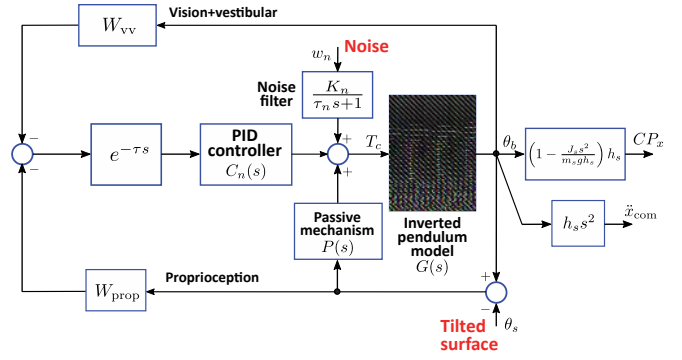


Fig. 3. Block diagram of the human postural neural balance control model.

A colored noise is denoted as a filtering mechanism with white noise  $w_n(t) \sim \mathcal{N}(0, 1)$  with low-pass filter  $\frac{K_n}{\tau_n s + 1}$ . From the neural balance control, we obtain the applied torque  $T_c$  as

$$T_c = \left(K_p + K_d s + \frac{K_i}{s}\right) e^{-\tau s} (W_{\text{prop}} \theta_s - \theta_b) + K_{ps} (\theta_b - \theta_s) + \frac{K_n}{\tau_n s + 1} w_n, \quad (4)$$

where we use model property  $W_{\text{vv}} + W_{\text{prop}} = 1$  from [5].

#### B. Model Parameter Estimation

To estimate the model parameters, we need to compute the transfer function from  $w_n(t)$  to outputs such as  $CP_x$  and  $a_x := \ddot{x}_{\text{com}}$ , which are measured by the force plates and the accelerometer on the upper body, respectively. From (1) to (4), we obtain

$$CP_x = \left(h_s + \frac{J_s s^2}{m_s g}\right) \theta_b, \quad a_x = h_s s^2 \theta_b, \quad (5)$$

where  $\theta_b = G_{w_n}(s) w_n + G_{\theta_s}(s) \theta_s$ ,

$$G_{w_n}(s) = \frac{K_n}{(\tau_n s + 1) \Phi(s)}, \quad G_{\theta_s}(s) = \frac{C_n(s) e^{-\tau s} - K_{ps}}{\Phi(s)},$$

and  $\Phi(s) = J_s s^2 - (m_s g h_s + K_{ps}) + C_n(s) e^{-\tau s}$ . We use the power spectrum of measured signal  $CP_x$  and  $a_x$  to estimate the model parameters. From (5), the power spectrum  $S_{CP_x}(\omega)$  and  $S_{a_x}(\omega)$  are given as

$$S_{CP_x}(\omega) = \left(h_s^2 + \frac{J_s \omega^2}{m_s g}\right) \|G_{w_n}(\omega)\|^2, \quad (6)$$

$$S_{a_x} = h_s \omega^2 \|G_{w_n}(\omega)\|^2. \quad (7)$$

Similar to the approach in [5] and [6], the model parameters are obtained by minimizing the following weighted errors between the model prediction and experimental data at a selective frequencies, namely,

$$E = \sum_{i=1}^N \left| \frac{S_{CP_x}(\omega_i) - S_{CP_x}^{exp}(\omega_i)}{S_{CP_x}^{exp}(\omega_i)} \right| + r \left| \frac{S_{a_x}(\omega_i) - S_{a_x}^{exp}(\omega_i)}{S_{a_x}^{exp}(\omega_i)} \right|,$$

where  $S_{CP_x}(\omega_i)$  ( $S_{a_x}(\omega_i)$ ) and  $S_{CP_x}^{exp}(\omega_i)$  ( $S_{a_x}^{exp}(\omega_i)$ ) are the model-predicted and experimental power spectrum for  $CP_x$  ( $a_x$ ) signals at frequency  $\omega_i$ , respectively,  $N$  is the total

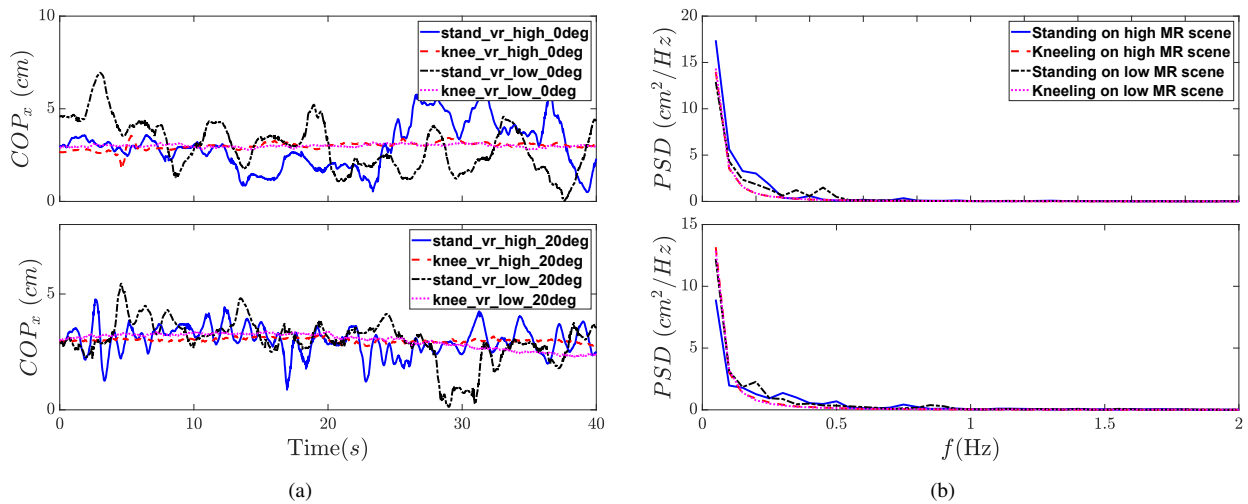


Fig. 4. (a) COP in A-P direction of subject 2. (b) Power spectral density of experimental  $CP_x$  results averaged across all the subjects. As shown are results for standing and kneeling tests on level (0 deg, top figure) and sloped surface (20 deg, bottom figure) for low and high elevated MR scene.

number of selected frequencies, and  $r > 0$  is a weight factor. To simplify the optimization process, we set weight constant  $r$  to be 0. In each optimization step, Fréchet distance was calculated between the simulated and the experimental PSDs.

#### IV. EXPERIMENTAL RESULTS

Fig. 4(a) shows the variation of the normalized  $CP_x$  during postural sway of one subject. Larger signal variations are clearly observed during stance on level or sloped surface, while variations during kneeling remain small. Fig. 4(b) shows the results of the PSD of the  $CP_x$  experimental data for stance and kneeling tests. The results are averaged across all the subjects for test conditions on level (0 deg) and sloped surface (20 deg) for low and high elevated MR scenes. Stance on level surface with shown low or high altitude MR scenes exhibit higher spectral density values compared to the ones observed during kneeling, regardless of the displayed visual scenes, see top figure of Fig. 4(b).

Comparing PSD of  $CP_x$  during stance on level surface (0 deg) shows higher values at frequencies below 0.3 Hz and higher area under the curve, when subjects were shown high elevated surface. These observations suggest less postural sway when observing high elevation visual scenes. Contrary, the higher PSD values of  $CP_x$  at frequencies between 0.3 and 0.6 Hz are observed when subjects were shown low level scene environment. The PSD results of  $CP_x$  for kneeling on the 20 deg sloped surface show similar trends as those observed on level surface. Surprisingly, the mean spectral density during stance on the 20 deg sloped condition exhibit lower values and lower area under the curve for frequencies below 0.3 Hz and higher area under the curve for frequencies between 0.3 to 0.6 Hz. These results suggest less sway during stance on a sloped surface with the visual stimulus of high elevation working environment. This could be the result of the subjects applying corrective reactions to reduce sway and increase postural stability.

Fig. 5(a) shows the average results of the RMS of  $CP_x$  signals across all subjects. Higher RMS during all stance trials indicate higher variability in magnitude of the  $CP_x$  compared to all kneeling trials. Comparing RMS values during stance and kneeling trials individually, the results show the lowest RMS values during postural balance when high MR elevation scene was shown to the subjects. Observations of less postural sway of subjects during those trials imply that the subjects restricted their sway at high elevation as a consequence of the presence of a visual threat. The average results across all subjects of mean velocities of  $CP_x$  signal in Fig. 5(b) show higher values during stance compared to kneeling across all test conditions. The comparison of mean velocity values among kneeling trials, shows the highest mean velocity during kneeling on a flat surface with low MR environment scene. During stance, mean velocities of  $CP_x$  increase with increase of the slope of the supporting surface regardless of the displayed low/high environmental scene. The results of the normalized torques exerted on the force plate during postural balance are shown in Fig. 5(c). All normalized torque values during kneeling are lower compared to those during stance across same test conditions. Normalized torques during stance or kneeling on 20 deg sloped surface exhibit the lowest values across all test conditions.

Fig. 6 shows the trunk linear accelerations in A-P and M-L directions during postural balance. The major axes with variance of the 95% ellipse of the postural sway accelerations are shown in Fig. 5(d). The smallest ellipse (i.e., major and minor axes) of the postural sway accelerations is observed during kneeling with shown low elevation in the MR immersion environment. These observations are hold for both level and sloped surface conditions. Contrary, the largest deviation across all tests is surprisingly for the kneeling tests with the high immersion environment on both level and sloped surfaces.

Optimization process of model parameters was performed for the individual test of each subject. Figs. 7(a) and 7(b)

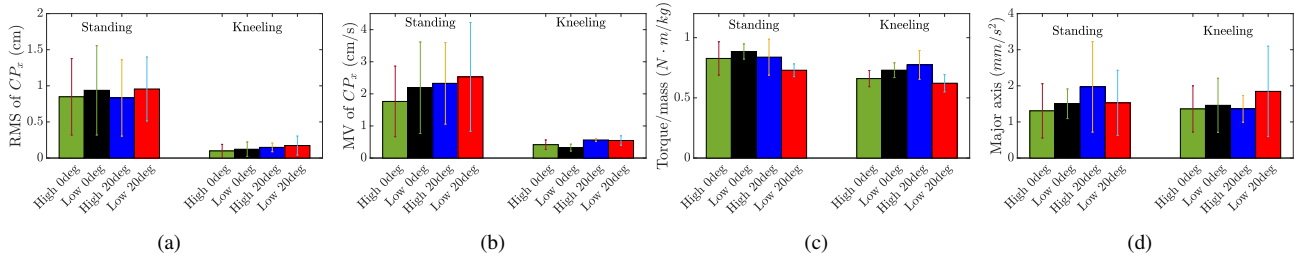


Fig. 5. Results from standing and kneeling trials under various test condition with averaged values across all subjects of (a) average RMS of  $CP_x$ , (b) average MV of  $CP_x$ , (c) normalized torque values, and (d) major axis of the 95% ellipse of linear acceleration sway.

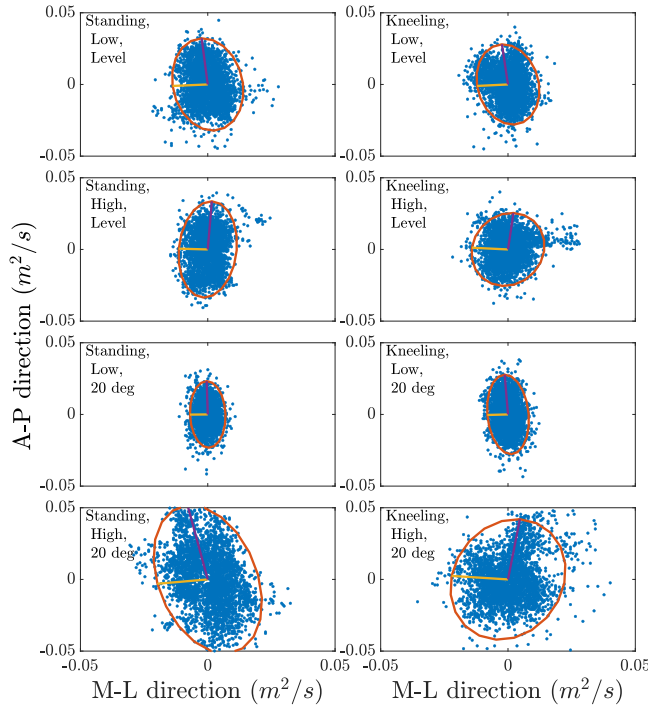


Fig. 6. Results of the 95% ellipse of trunk linear accelerations in A-P and M-L directions during postural balance shown for all test conditions during kneeling and standing.

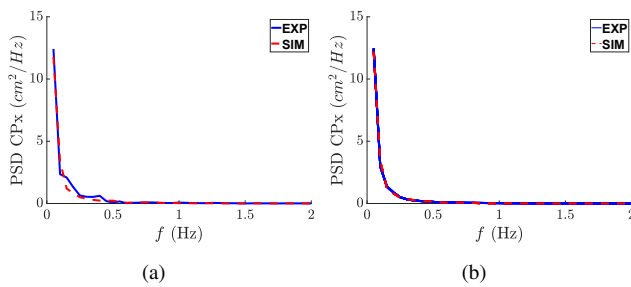


Fig. 7. Comparison of the experimental and matching model prediction results of the PSD of  $CP_x$  for a) standing on 20 deg slope with low VR scene, b) kneeling on 20 deg slope with high VR scene.

show close matching between the PSD of the experimental and model prediction  $CP_x$  results for stance and kneeling tests, respectively. Both figures present results of one subject on level and sloped surfaces with low and high MR environmental scenes.

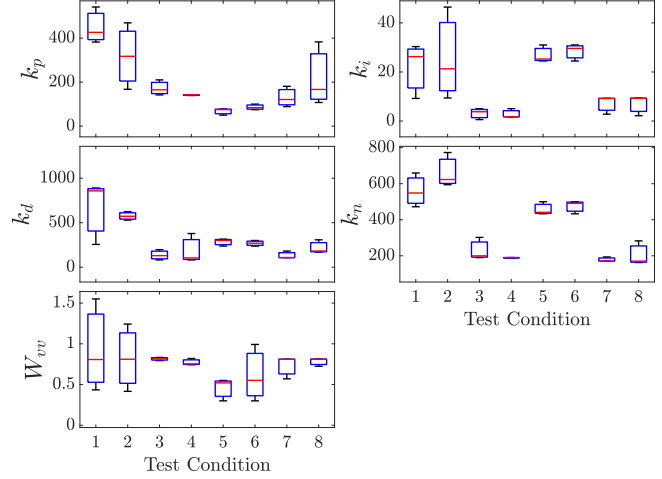


Fig. 8. The parameters of standing and kneeling gaits were identified from simulation using the proportional-derivative neural controller. 8 test conditions are included as standing (condition 1 ~ 4) and kneeling (condition 5 ~ 8): Low, level surface; High, level surface; Low, 20 deg slope surface; High, 20 deg slope surface.

TABLE I  
OPTIMIZATION PARAMETERS FOR ALL THE SIMULATED CONDITIONS.

	$k_p$	$k_i$	$k_d$	$k_n$	$W_{vv}$
Standing, Low, Level surface	449.8	21.9	667.6	560.0	0.93
Standing, High, Level surface	318.0	25.7	575.1	663.5	0.82
Standing, Low, 20 deg slope	172.4	3.1	136.1	230.5	0.82
Standing, High, 20 deg slope	141.2	2.8	188.1	189.0	0.77
Kneeling, Low, Level surface	67.6	26.9	284.0	458.2	0.46
Kneeling, High, Level surface	86.3	28.4	269.0	474.6	0.61
Kneeling, Low, 20 deg slope	130.3	7.1	132.0	178.1	0.73
Kneeling, High, 20 deg slope	218.9	6.9	219.6	205.2	0.78

For the individual simulation condition, the model parameters of the neural control were obtained by optimization described in Section III-B. Summary of the tuned model coefficients and their distributions for all the subjects obtained from the optimization is shown in Fig. 8 and Table I. Parameter optimization of the stance tests shows a greater proportional control gain ( $k_p$ ) on level surface than sloped surface while kneeling tests shows an opposite trend. A clear and consistent increased trend is shown for the integral gain ( $k_i$ ) on level surface compared to the ones used for the sloped surface. Control parameter  $k_d$  and  $k_n$  exhibit a similar trend as that of the  $k_i$ , with increased values for trials on the level

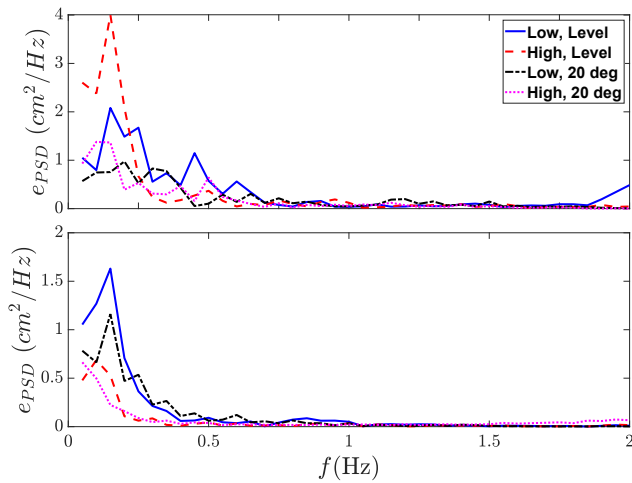


Fig. 9. The error curves between experimental and simulated PSD plots are presented for both standing (top) and kneeling (bottom) gaits in various test conditions.

surface and one fold or two smaller values for trials on the 20 deg sloped surface. Lastly, the coefficients related to visual and vestibular sensory feedback  $W_{vv}$  are all within a range above 0.7 except kneeling on level surface tests.

Fig. 9 shows that parameter optimization of kneeling tests has smaller errors than stance tests in general, which indicates the proposed model has a better fit for kneeling gaits. For the optimization of stance tests, smaller error from experiments on the sloped surface than on the level surface is observed especially at lower frequency range. The error plots of kneeling tests show smaller values in the high elevated MR scenes than those under low elevated scenes.

Our results on kneeling tests show the subjects have a larger variance of center of pressure on both level and slope surfaces in the A-P direction. This suggests that subjects are more relax on low/ground level surface than on the elevated surface. On the high elevation scene, the normalized torque has higher variance, which indicates that subjects used more variant torques to control their balance. The power spectral density and RMS of center of pressure curves matches with the results of previous study [6]. Comparison of center of pressure mean velocities showed several times higher values during stance than kneeling. These results contradict findings from previous study [6], where surprisingly a reverse trend was reported. The value of control gains  $k_p$  and  $k_d$  show similar decreasing trend as in [6] from stance to kneeling, however the noise gain  $k_n$  doesn't agree with the results, which also shows a decreasing trend in [6]. A small sample size might affect our results.

## V. CONCLUSION

In this paper, we investigated the postural balance during kneeling and standing on sloped and elevated surfaces. A postural model was developed to simulate postural sway in the anterior-posterior direction. The model and controller parameters were optimized to precisely match the experimental results. Variation of model parameters with respect to

particular test conditions provided insight on relationship on human neural balance postural control and sensory system. This work complements the existing research on the postural control during kneeling, which is of particular relevance for construction workers that commonly perform work on elevated and inclined surfaces.

## REFERENCES

- [1] Bureau of Labor Statistics, "National Census of Fatal Occupational Injuries in 2019," Bureau of Labor Statistics, Washington, DC, Tech. Rep., 2020.
- [2] H. Hsiao and P. Simeonov, "Preventing falls from roofs: A critical review," *Ergonomics*, vol. 44, no. 5, pp. 537–561, 2001.
- [3] X. Dong, X. Wang, and R. Katz, *The Construction Chart Book – The U.S. Construction Industry and Its Workers*, 6th ed. Silver Spring, MD: CPWR, 2018.
- [4] D. A. Winter, A. E. Patla, F. Prince, M. Ishac, and K. Gielo-Periczak, "Stiffness control of balance in quiet standing," *J. Neurophysiol.*, vol. 80, pp. 1211–1221, 1998.
- [5] R. J. Peterka, C. F. Murchison, L. Parrington, P. C. Fino, and L. A. King, "Implementation of a central sensorimotor integration test for characterization of human balance control during stance," *Front. Neurology*, vol. 9, 2018, article 1045.
- [6] R. A. Mezzarane and A. F. Kohn, "Postural control during kneeling," *Exp. Brain Res.*, vol. 187, pp. 395–405, 2008.
- [7] A. Bhattacharya, P. Succop, L. Kincl, M. L. Lu, and A. Bagchee, "Postural stability during task performance on elevated and/or inclined surfaces," *Occup. Ergon.*, vol. 3, pp. 83–97, 2002/2003.
- [8] P. I. Simeonov, H. Hsiao, B. W. Dotson, and D. E. Ammons, "Control and perception of balance at elevated and sloped surfaces," *Human Factors*, vol. 45, no. 1, pp. 136–147, 2003.
- [9] T. W. Cleworth, B. C. Horslen, and M. G. Carpenter, "Influence of real and virtual heights on standing balance," *Gait Posture*, vol. 36, pp. 172–176, 2012.
- [10] H. Hsiao, P. Simeonov, B. Dotson, D. Ammons, T.-Y. Kau, and S. Chiou, "Human responses to augmented virtual scaffolding models," *Ergonomics*, vol. 48, no. 10, pp. 1223–1242, 2005.
- [11] F. Bosché, M. Abdel-Wahab, and L. Carozza, "Towards a mixed reality system for construction trade training," *J. Comput. Civ. Eng.*, vol. 30, no. 2, 2016, article 04015016.
- [12] X. Li and W. Yi and H.-L. Chi and X. Wang and A. P. C. Chan, "A critical review of virtual and augmented reality (VR/AR) applications in construction safety," *Automat. Constr.*, vol. 86, pp. 150–162, 2018.
- [13] J. M. D. Delgado, L. Oyedele, T. Beach, and P. Demian, "Augmented and virtual reality in construction: Drivers and limitations for industry adoption," *J. Constr. Eng. Manage.*, vol. 146, no. 7, 2020, article 04020079.
- [14] I. Okpala, C. Nnaji, and A. A. Karakhan, "Utilizing emerging technologies for construction safety risk mitigation," *Pract. Period. Struct. Des. Constr.*, vol. 25, no. 2, 2020, article 04020002.
- [15] Y. Shi, J. Du, C. R. Ahn, and E. Ragan, "Impact assessment of reinforced learning methods on construction workers' fall risk behavior using virtual reality," *Automat. Constr.*, vol. 104, pp. 197–214, 2019.
- [16] S. Yu, T.-H. Huang, X. Yang, C. Jiao, J. Yang, H. Hu, S. Zhang, Y. Chen, J. Yi, and H. Su, "Quasi-direct drive actuation for a lightweight hip exoskeleton with high backdrivability and high bandwidth," *IEEE/ASME Trans. Mechatronics*, vol. 25, no. 4, pp. 1794–1802, 2020.
- [17] S. Chen, D. T. Stevenson, S. Yu, M. Mioskowska, J. Yi, H. Su, and M. Trkov, "Wearable knee assistive devices for kneeling tasks in construction," *IEEE/ASME Trans. Mechatronics*, 2021.
- [18] K. Hunte, S. Chen, J. Yi, and H. Su, "Assist-as-needed control of a wearable lightweight knee robotic device," in *Proc. IEEE/ASME Int. Conf. Adv. Intelli. Mechatronics*, Boston, MA, 2020, pp. 1477–1482.
- [19] S. Chen, S. S. Bangaru, T. Yigit, M. Trkov, C. Wang, and J. Yi, "Real-time walking gait estimation for construction workers using a single wearable inertial measurement unit (imu)," in *Proc. IEEE/ASME Int. Conf. Adv. Intelli. Mechatronics*, Delft, Netherlands, 2021.
- [20] A. J. Solomon, J. V. Jacobs, K. V. Lomond, and S. M. Henry, "Detection of postural sway abnormalities by wireless inertial sensors in minimally disabled patients with multiple sclerosis: a case-control study," *J. Neuroeng. Rehab.*, vol. 12, no. 1, pp. 1–9, 2015.